Cluster-Based Semi-Empirical Model for Dopant Activation in Silicon Carbide

Balazs Bamer[1]*, Sabine Leroch[1], Andreas Hössinger[2], and Lado Filipovic[1]
[1]Christian Doppler Laboratory for Multi-Scale Process Modeling of Semiconductor Devices and Sensors,
Institute for Microelectronics, TU Wien, 1040 Vienna, Austria
[2]Silvaco Europe Ltd., St Ives, Cambridgeshire, PE27 5JL, United Kingdom
*Email: bamer@iue.tuwien.ac.at

2024 International Conference on Simulation of Semiconductor Processes and Devices (SISPAD) | 979-8-3315-1635-2/24/$31.00 ©2024 IEEE | DOI: 10.1109/SISPAD62626.2024.10732978

***Abstract*—We present a cluster-based semi-empirical model for dopant activation in silicon carbide (SiC). We model the following species: dopants on lattice points, point defects, dopant-defect pairs, and small clusters of different sizes. We define the possible reactions between these species, add their reaction kinetics, and use a system of ordinary differential equations (ODEs) to model the time evolution of the concentration of the different species during annealing. We use the MaxLIPO+TR optimizer to obtain the post-implant conditions of the SiC film, including the various cluster concentrations. These concentrations are not measurable and can only be calculated through time-intensive atomistic simulations, which we apply to verify and calibrate our model. The framework presented here, consisting of an ODE model generator, an ODE solver and an optimizer, gives a practical solution to predict as-implanted defect concentrations, which is missing from previous works.**

***Index Terms*—Silicon carbide, ion implantation, annealing, dopant activation, nanoscale clusters, process simulation**

I. Introduction

The primary means to introduce a dopant in semiconductors today is through ion implantation, which allows for precise control of the doped region depth and concentration. Its main drawback is its induced damage to the semiconductor crystal structure. This damage weakens the semiconductor's electrical properties by making some dopant atoms electrically inactive. Inactive dopant atoms combine in smaller or bigger clusters instead of residing in desired lattice positions. This change of properties depends on the ion flux, energy, and implantation temperature. Subsequent processing steps, like annealing, can repair the crystal structure and activate the dopant atoms. Depending on the damage caused by ion implantation, the semiconductor, such as silicon carbide (SiC), may require temperatures as high as 2000°C during annealing. Physical simulations may reveal that a lower temperature or shorter annealing time might be sufficient when the added effect of subsequent processing steps like thermal oxidation can also be considered. An important property of ion-implanted semiconductors is the activation ratio, which we address in this work. It is defined as the ratio of electrically active dopant atoms to the total implanted dopant amount.

Wendler et al. [1] have shown that, depending on the implant species, dose, and temperature, the damage in SiC is in the form of point defects, clusters of different sizes, and partially or fully amorphous regions. Weber et al. [2] has simulated primary knock-on atoms (PKAs) of C, Si, and Au irradiations with energies up to $50\,\mathrm{keV}$. They have found that most clusters resulting from Si irradiation contained only up to 4 interstitials. Therefore, we restrict our investigation to small clusters since ion implantation in SiC is performed with light ions (B, Al, N, and P) [3].

Since silicon has been used in microelectronics for many decades, there is significantly more information on Si doping and cluster-based modelling when compared to SiC. Stiebel et al. [4] propose a larger model for Si doping consisting of 9 cluster species and a smaller one with only 4 cluster species, together with the applied reaction rates. Yoo et al. [5] use binding energies from theoretical and experimental works on a similar set of small cluster species up to B_4I_2. Kwok et al. [6] use maximum likelihood and maximum *a posteriori* estimations of results from density functional theory (DFT) simulations and experiments to derive physical parameters for clusters with sizes of up to 7 atoms. They did not distinguish the exact composition of mixed boron-silicon clusters of the same size. Although most authors agree that only small clusters considerably impact dopant activation, Aboy et al. [7] showed some crucial effects of larger clusters. They have demonstrated that mixed clusters with up to 9 boron and silicon atoms can impact boron activation when using high doping concentrations.

II. Model Design

Our model is based on an established cluster-based model for dopant activation in silicon [8]. We simulate the following species in our model for boron activation in SiC:

- Point defects: interstitials and vacancies
- Dopant-defect pairs: $\mathrm{XInt_A}$ and $\mathrm{XVac_A}$
- Loose active dopant: $\mathrm{X_{LA}}$
- Dopant-interstitial clusters like $\mathrm{X_2Int_3}$

We neglect the difference between C and Si interstitials and vacancies and model the following types of reactions:

- Point defect recombination: $\mathrm{Int} + \mathrm{Vac} \longleftrightarrow 0$
- Pair and point defect interaction: $\mathrm{XInt_A} + \mathrm{Vac} \longleftrightarrow \mathrm{X_{LA}}$
- Dopant defect cluster formation and dissolution: $\mathrm{Int} + \mathrm{XInt_A} \longleftrightarrow \mathrm{X_1Int_2}$

Through the simulation, we assume that the high-speed processes, like part of the point defect recombination, which is

in the order of less than one millisecond, are already completed as our timescale of simulation is several orders of magnitude longer, in the order of seconds. We concentrate our model on elementary second-order reactions [9, Chapter 6] which poses a practical limit on the number of species in the modelled system because optimizing for more than dozens of initial concentrations (with at least as many ODEs) would not be feasible. Therefore, we use this general form of reaction rates for a reaction X + Y $\longleftrightarrow$ Z:

- has a forward rate $R_f = C_X C_Y K_f$
- and a backward rate $R_r = C_Z K_r$
- Backward rate for point defect recombination is a special case: $R_r = C_{X,eq} C_{Y,eq} K_r$

We have chosen to model the time evolution of the species in a continuum model, so the species are modelled by their continuous concentrations. Diffusion and reactions between the species influence the time evolution of the concentrations at any point. The reactions are modelled using a system of ODEs influenced by their forward and backward rates. Using the above notations, the system of ODEs can be written as:

$$\frac{\partial C_X}{\partial t} = \sum_{i \in M_X} R_{f_i} - \sum_{j \in N_X} R_{r_j}$$

for each species X in the system, where M_X is the set of reactions producing X and N_X is the set of reactions consuming X.

III. Choice of Optimizer Algorithm

To solve the set of ODEs which describe the activation, the reaction rates and initial concentration of species and clusters are required. Here, *initial concentrations* refer to concentrations after ion implantation, eventually also considering a very short annealing time. The reaction rates can be computed using point defect equilibrium concentrations, mobile species diffusivity coefficients, activation energies, crystal lattice constant, and auxiliary coefficients. These values are either known from the literature or can be estimated using *ab-initio* DFT and molecular dynamics (MD) simulations.

We can indirectly assess the initial concentrations of point defects and some cluster species if we have sufficient data from activation measurements or atomistic simulations before and after annealing with well-defined process conditions. Moreover, some missing parameters for the reaction rates can also be estimated. One way to find these values is by using an optimizer.

Here, using a first guess for initial concentrations and parameters, the ODE system is solved for a well-defined annealing time, or until a steady-state solution is reached. Then, the difference between the calculated and the measured activation ratio gives the error of this evaluation. We can use an optimizer to systematically tune the free parameters and use the evaluation error as feedback for the optimization process. This task is then a multi-variable single-objective optimization problem.

For the ODE solver, we use the Sundials CVODE library with a dense solver method and the BDF multistep method [10], [11]. For the optimization problem, we have chosen Dlib's *MaxLIPO+TR* global optimizer [12], [13]. An advantage of this optimizer over alternatives, like Bayesian optimization, is that it does not require tuning hyperparameters. As we have a complex optimization problem with several dozens of dimensions, MaxLIPO+TR is also superior to gradient-based optimizers.

The Dlib global optimizer assumes that the function to optimize for is Lipschitz-continuous. For the 1D case this must hold $|f(x_1) - f(x_2)| <= k|x_1 - x_2|$ for all $x_1, x_2 \in$ some interval, where $f(x)$ is the function to optimize for. The key idea is maintaining the function's piecewise linear upper bound using the evaluated points: $U(x) = \max_{i=1..t} (\mathrm{f(x_i)} + \mathrm{k}\|\mathrm{x} - \mathrm{x_i}\|)$ where k is estimated in each turn.

The Dlib global optimizer first chooses points at random. Then, for every odd step, it sets the next point to sample: x_{t+1} where $U(x)$ is minimal. The function $f(x)$ is then evaluated here. For every even step, a Powell-style trust region search is performed using a quadratic approximation to find the local minimum.

Since the Dlib library uses hyperrectangle search space, and some dimensions are concentrations, out of the box, it would search for concentration combinations which would not satisfy physical constraints like doping. Therefore, the library was modified to include restraints to ensure a physically feasible search space.

IV. Optimizer Design

To test the framework and the optimization process, we use the empirical target function shown in Fig. 1 from Šimonka's PhD thesis [14]. The function approximates the boron activation ratio as a function of annealing temperature and doping concentration. Fig. 1 shows experimental results as colour dots from [15]. We use this model as a target for our optimizer. Instead of optimizing initial concentrations for various temperature-doping pairs individually, we pick an annealing temperature and search the initial concentrations as functions of doping concentrations (black dots in Fig.1). We suspect that by having many temperature-dependent parameters in the system, using the optimized values for other temperatures may give a good approximation.

We have chosen cubic natural splines as the functions describing each initial concentration because these have intuitive behaviour as we move the control nodes. The control nodes' X coordinates are fixed using a geometric progression across the concentration domain of interest, cf. Fig. 2. The Y coordinates represent concentrations with a wide dynamic range, so the optimizer and the splines use the natural logarithm of the concentrations for optimal behaviour. The optimizer then looks for the Y coordinates within the search space. We have found that four control nodes are sufficient for a good fit. The concentration domain of interest is the domain for a given temperature, where the activation ratio is within the interval $(0.1, 0.9)$.

Splines tend to overshoot the bounds when one control node is near the bound and an adjacent one is further away. In our

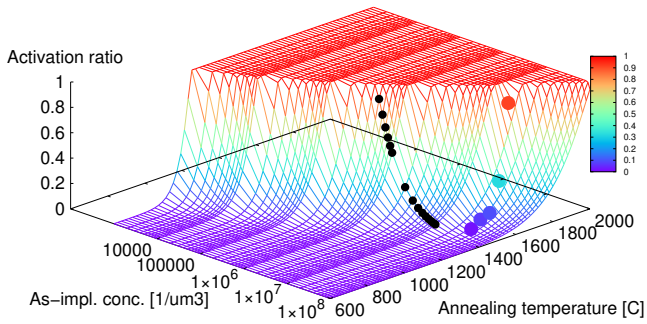

Figure 1: Electrical activation as a function of the total concentration and annealing temperature for B-implanted SiC. The grid represents the empirical function, the colour points are experimental data, and the black points are our optimization target (see text).

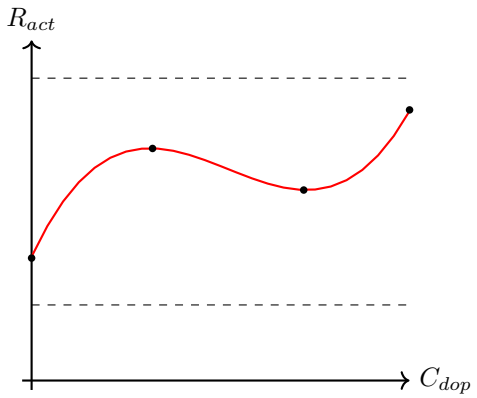

Figure 2: A spline within bounds with four control nodes.

case, this could result in a nonphysical concentration value, so we have developed an algorithm to slightly adjust control nodes, causing overshoot while preserving the spline's form. The splines' control nodes at a given doping concentration represent a valid initial concentration setting, including the desired initial activation ratio. However, as the interpolation is based on the logarithm of the concentrations, taking the exponential of the interpolated values does not add up to the desired doping or initial active concentrations. Therefore, we calculate the total active and cluster concentrations and normalize each interpolated concentration to allow these totals to have the desired value. The optimizer needs to calculate the error in each iteration, cf. Fig. 4. This is done in several sample points whose concentrations can be given manually or allow the application to calculate them similarly to the spline control points. With a dense enough sample point set, the optimizer can consider every part of the splines in its decisions, cf. Fig. 3. The aggregated error value is calculated using $E = \sum_i (\log A_{act_i} - \log A_{targ_i})^2$.

Simulations show that an independent four-control node spline per species gives too many degrees of freedom, resulting in extreme waviness of the splines, suggesting likely nonphysical behaviour. To overcome this, we penalize waviness by summing the relative changes of the node's Y coordinates and adding these sums to the above-mentioned error.

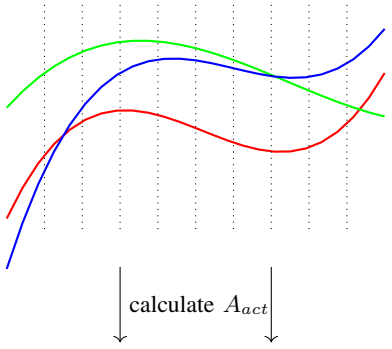

Figure 3: error is evaluated at a denser sample point set than the spline control nodes.

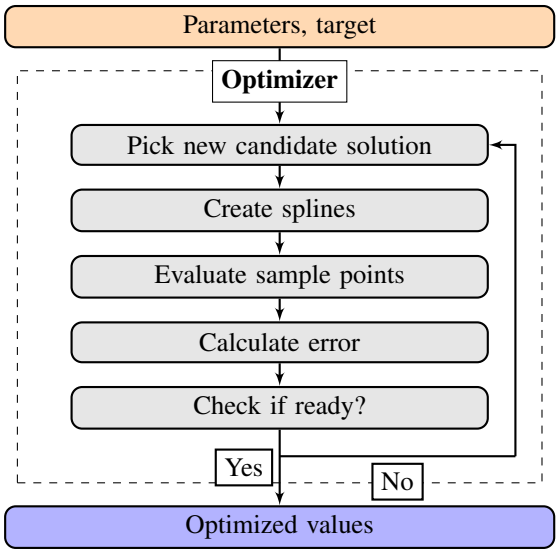

Figure 4: Optimizer workflow.

We have designed the optimizer to find the missing reaction rates (forward, reverse, or both). These are modelled to be concentration-independent, so each unknown rate requires only one more dimension in the search space. We have developed a model generator to help investigate various cluster configurations, species reactions and model parameters.

V. Results

We use the black dots corresponding to annealing at 1400 °C in Fig.1 as the optimization target. We have decided to use the 4 cluster species in the model: B_1Int_2, B_2, B_2Int_1 and B_2Int_2. Since we do not have the cluster activation energies for SiC, we also used the optimizer to obtain the missing reaction rates. Fig. 5 shows the splines representing the initial concentration of each species as a function of doping

concentration. The plot range has been selected such that the target activation ratio ranges from 0.06 to 0.95. We have chosen the initial activation ratio to be uniformly 0.05, cf. Fig. 6.

This model shows an almost perfect fit with the optimization target. It consists of the estimated reaction rates and the functions of species' initial concentrations versus doping concentration.

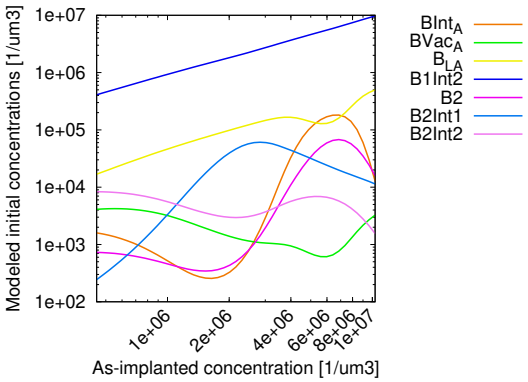

Figure 5: Splines describing the initial concentrations of each species vs doping concentration when annealing at $1400\,^{\circ}\mathrm{C}$

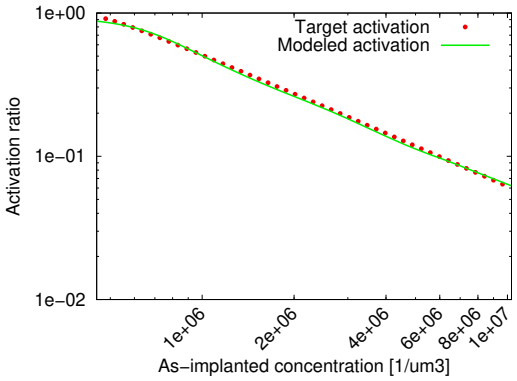

Figure 6: Target (red) and modelled (green) activation ratio vs doping concentration when annealing at $1400\,^{\circ}\mathrm{C}$.

VI. Conclusion

We have developed a semi-empirical cluster model for dopant activation in silicon carbide and an optimizer application to determine the initial concentrations of the defect species present in the material after ion implantation. The optimizer can obtain the initial concentrations as functions of the as-implanted concentrations for a specific annealing temperature. It enables us to obtain values for physical as well as fitting parameters, which are difficult to obtain experimentally.

Acknowledgment

Financial support by the Federal Ministry of Labour and Economy, the National Foundation for Research, Technology and Development, and the Christian Doppler Research Association is gratefully acknowledged.

References

[1] E. Wendler, A. Heft, and W. Wesch, "Ion-beam induced damage and annealing behaviour in sic," *Nucl. Instr. and Methods in Phys. Research*, vol. 141, no. 1, pp. 105–117, 1998. DOI: 10.1016/S0168-583X(98)00083-4.

[2] W. Weber, F. Gao, R. Devanathan, W. Jiang, and C. Wang, "Ion-beam induced defects and nanoscale amorphous clusters in silicon carbide," *Nucl. Instr. and Methods in Phys. Research*, vol. 216, pp. 25–35, 2004. DOI: 10.1016/j.nimb.2003.11.016.

[3] Roccaforte *et al.*, "Selective doping in silicon carbide power devices," *Materials*, vol. 14, no. 14, 2021. DOI: 10.3390/ma14143923.

[4] D. Stiebel, P. Pichler, and H. Ryssel, "On the influence of boron-interstitial complexes on transient enhanced diffusion," *MRS Proceedings*, vol. 568, p. 141, 1999. DOI: 10.1557/PROC-568-141.

[5] J. H. Yoo, C. O. Hwang, B. J. Kim, and T. Won, "Simple atomistic modeling of dominant b m i n clusters in boron diffusion," *Molecular Simulation*, vol. 31, no. 12, pp. 817–824, 2005. DOI: 10.1080/08927020500314118.

[6] C. T. M. Kwok, R. D. Braatz, S. Paul, W. Lerch, and E. G. Seebauer, *AIChE Journal*, vol. 56, no. 2, pp. 515–521, 2010. DOI: 10.1002/aic.11984.

[7] M. Aboy, L. Pelaz, E. Bruno, S. Mirabella, and S. Boninelli, "Kinetics of large B clusters in crystalline and preamorphized silicon," *Journal of Applied Physics*, vol. 110, no. 7, p. 073 524, Oct. 2011. DOI: 10.1063/1.3639280.

[8] K. Suzuki, T. Miyashita, Y. Tada, A. Hoefler, N. Strecker, and W. Fichtner, "Damage calibration concept and novel b cluster reaction model for b transient enhanced diffusion over thermal process range from 600/spl deg/c (839 h) to 1100/spl deg/c (5 s) with various ion implantation doses and energies," in *Int Electron Devices Meeting Techn. Digest*, 1997, pp. 501–504. DOI: 10.1109/IEDM.1997.650433.

[9] A. Hofmann, *Physical chemistry essentials*, eng. Cham: Springer, 2018, ISBN: 3319741667.

[10] Gardner *et al.*, "Enabling new flexibility in the SUNDIALS suite of nonlinear and differential/algebraic equation solvers," *ACM TOMS*, 2022. DOI: 10.1145/3539801.

[11] Hindmarsh *et al.*, "SUNDIALS: Suite of nonlinear and differential/algebraic equation solvers," *ACM TOMS*, vol. 31, no. 3, pp. 363–396, 2005. DOI: 10.1145/1089014.1089020.

[12] C. Malherbe and N. Vayatis, *Global optimization of Lipschitz functions*, Aug. 2017.

[13] D. E. King, "Dlib-ml: A machine learning toolkit," *Journal of Machine Learning Research*, vol. 10, no. 60, pp. 1755–1758, 2009. [Online]. Available: http://jmlr.org/papers/v10/king09a.html.

[14] V. Šimonka, "Thermal oxidation and dopant activation of silicon carbide," Ph.D. dissertation, TU Wien, Vienna, Austria, 2018. DOI: 10.34726/hss.2018.60302.

[15] F. Roccaforte, F. Giannazzo, and G. Greco, "Ion implantation doping in silicon carbide and gallium nitride electronic devices," *Micro*, vol. 2, no. 1, pp. 23–53, 2022. DOI: 10.3390/micro2010002.